Process Variable Influence on Arc Temperature Distribution

Effects of shielding gas composition, electrode tip geometry, and arc current on the gas tungsten arc temperature distribution

BY J. F. KEY, J. W. CHAN, AND M. E. McILWAIN

Introduction

Prior physical measurements of the gas tungsten arc generally have been confined to steady-state temperature, heat transport, and composition measurements of an arc shielded by pure argon (Ref. 1-20). A more limited number of studies have been conducted for an arc shielded with pure helium (Ref. 8, 11, 13, 21-23).

Glickstein proposed a one-dimensional model for radial temperature distribution in argon-helium mixtures (Ref. 5). Ikonomov (Ref. 24) and Vucanovic (Ref. 25) calculated radial temperature distributions as a function of thermal conductivity of the gas mixture, thereby including any gas mixtures having a thermal conductivity in the range considered. The effect of cathode vertex angle was investigated by Petrie (Ref. 15), Shaw, (Ref. 18, 19) and Erokhin (Ref. 26). To date, however, there has been no experimental characterization of welding arcs shielded by mixtures of argon and helium or argon and hydrogen using a variety of electrode tip geometries either to verify proposed models or to explain the reported interrelated penetration effects of these variables (Ref. 27-31).

This paper discusses experimental measurements of the radial temperature distribution in the gas tungsten arc using a wide range of shielding gas mixtures. Each of these compositions was evaluated for two arc currents, two electrode geometries, and two anode materials. These measurements are contrasted with actual welding results and theoretical models in an attempt to further fundamental understanding of the gas tungsten arc welding (GTAW) process.

Based on a paper presented under the title of "Shielding Gas Composition and Electrode Geometry Influence on Arc Properties" at the 62nd Annual AWS Convention held in Cleveland, Ohio, during April 5-10, 1981.

J. F. KEY and J. W. CHAN are with EG&G Idaho, Inc., Idaho Falls, Idaho; and M. E. McILWAIN is with Geo-Centers, Inc., Upper Newton Falls, Massachusetts.

Experimental Methods

Welding Equipment and Procedures

A 150 ampere (A) power supply designed for mechanized pipe welding was used for most of the experiments; experiments at higher currents used a different 300 A power supply. A micropositioning x-y fixture was fabricated to hold a straight water-cooled torch as shown in Fig. 1. The torch had a gas lens and cup to provide laminar flow around a 2.38 mm (0.094 in.) diameter 2% thoriated tungsten electrode. The electrode tips were ground to 30 or 90 deg vertex angles with a 0.125 mm (0.005 in.) diameter truncation.

A water-cooled copper chill block was used as the anode in the first series of experiments for simplicity as well as correlation with prior investigations. Since arc voltage and arc length (distance between the tip of the electrode and the workpiece) cannot be varied independently as the gas composition is changed, the arc length was considered the more important variable and kept constant at 2.0 mm (0.08 in.) in this series. The 2.0 mm (0.08 in.) arc length is representative of current practice in mechanized GTAW.

To relate results to real welding conditions, a similar series of experiments was conducted over a molten pool of AISI 304 stainless steel. This material, in the form of pipe, was rotated on a specially designed positioner in a spiral motion such that the arc impinged on fresh material continuously. Since the elevation of the molten pool above the surface of the workpiece varied with gas composition, these experiments used automatic voltage control (AVC) to provide a nearly constant arc length of approximately 2.0 mm (0.08 in.). The voltage selected was dependent on gas composition.

The combinations of shielding gas, electrode geometry, current, and anode material used are shown in Table 1.

Diagnostic Measurements

Optics System Design and Spectral Intensity Measurements. Since temperature would be calculated from measured spectral intensities, an optics and detection system was designed that measured spectral line intensity as a function of time and position in the arc. Figure 2 is a schematic layout of the system shown in

Table 1—Experimental Matrix

Shielding gas composition, wt-%	Electrode vertex angle, deg	Current, A	Anode material[a]
100 Ar/0 He	30, 90	150, 300	Cu, 304 SS
90 Ar/10 He	30, 90	150, 300	Cu
75 Ar/25 He	30, 90	150, 300	Cu
50 Ar/50 He	30, 90	150, 300	Cu
25 Ar/75 He	30, 90	150, 300	Cu, 304 SS
10 Ar/90 He	30, 90	150, 300	Cu, 304 SS
95 Ar/5 H_2	30, 90	150, 300	Cu, 304 SS

(a) SS = stainless steel

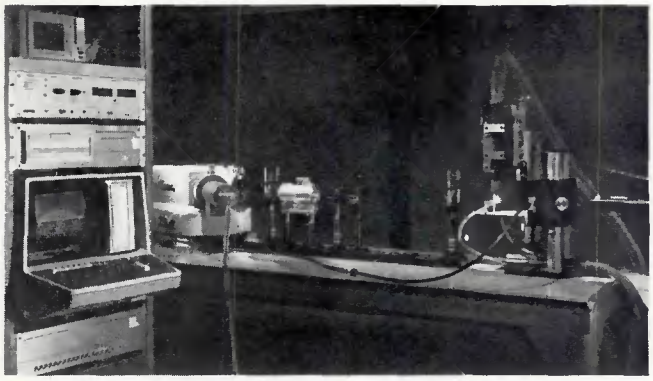

Fig. 1—Experimental equipment

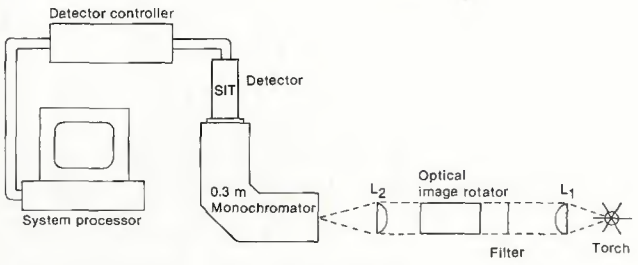

Fig. 2—Schematic layout of optics and OMA

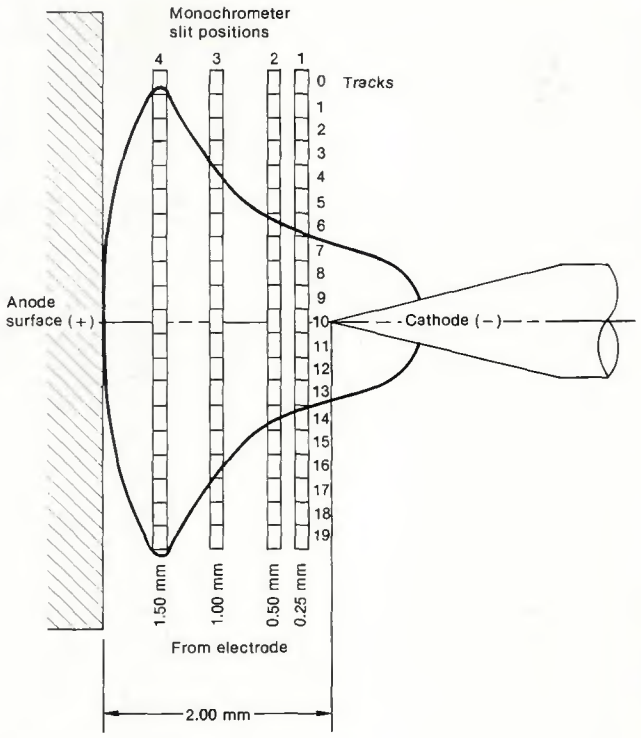

Fig. 3—Arc scanning matrix

Fig. 1 and employed for the temperature measurements. Light emerging from the arc was collimated by a 250 mm focal length glass lens (L_1). The collimated light was then filtered using a 25 nm bandpass filter centered at 450 nm. The filtered light passed through an image rotator, which rotated the image by 90 deg. The light passing from the rotator was then reimaged with another 250 mm (9.8 in.) lens (L_2) on the slits of a 0.3 m (11.8 in.) monochromator.

An optical multichannel analyzer (OMA)* consisting of a silicon intensified target (SIT) detector, a detector controller featuring programmable scan patterns, and a microcomputer-based processor was the principal measuring instrument. The detector was mounted at the exit focal plane of the monochromator and measured the intensity of spectrally dispersed light as a function of position on the target. The resulting signals from the SIT detector were analyzed and stored by the system processor and controller.

Figure 3 shows the scan pattern used for the intensity measurements. The arc was positioned on the slits in the positions shown. The OMA scanned a given slit in a sequential series of tracks. Each track scanned was a rectangle 0.01 × 0.25 mm (0.0004 × 0.01 in.) The 0.01 mm (0.0004 in.) dimension represents the maximum slit width and the 0.25 mm (0.01 in.) dimension the programmed track height. A 2.5 nm (9.8×10^{-11}in.) wide portion of the spectrum centered at 458.0 nm (18×10^{-9}in.) was recorded.

The image of the arc was positioned on the slits by first aligning a He-Ne laser parallel to the surface of the chill block such that the block obscured approximately half of the beam. The resulting image of the laser beam on the monochromator slits was adjusted to overlap the edge of the chill block shadow and the slit. The position of the arc image on the slit was then adjusted by translation stage adjustments to the desired measurement position. Four positions in the arc were routinely interrogated. These were 0.25, 0.50, 1.00, and 1.50 mm (0.0098, 0.02, 0.04, and 0.059 in.) from the tip of the tungsten electrode.

Arc spectra were obtained by accumulating 10 sequential scans of the detector. Although scanning rate was programmable, a rate of 1 ms/track was used throughout these experiments. The resulting spectra initially were analyzed manually to find the desired peak. Peak values were obtained after background subtraction. The resulting peak values were input to a computer program to yield plasma temperatures.

A computerized peak search program is used now instead of manual analysis. The data are automatically entered into the temperature calculation program. Each measurement is repeated five times and averaged.

Temperature Calculation. In order to calculate Ar II plasma temperatures, the two-line method was used (Ref. 32). A computer program was used to deconvolute the line-of-sight measured intensities to obtain a spacially resolved distribution of intensities. The Abel inversion (Ref. 33) was used to evaluate the radial intensities using the following equation:

$$\epsilon(r) = -\frac{1}{\pi}\int_{r}^{r_0} \frac{I(y)\,dy}{(y^2-r^2)^{1/2}}$$

where $\epsilon(r)$ is the radial intensity for element r, and I is the line-of-sight change in measured intensity along the image. After the radial intensities were computed, the plasma temperature for each radial segment was determined using:

$$\frac{\epsilon(r)_1}{\epsilon(r)_2} = \frac{A_1 g_1 \lambda_2}{A_2 g_2 \lambda_1} \exp\left[\frac{E_2 - E_1}{kT}\right]$$

where $\epsilon(r)_1$ is the radial intensity for the 457.9 nm line, $\epsilon(r)_2$ is the radial intensity for the 458.99 nm line, A is the transition probability, g is the level degeneracy, λ is the wavelength, and E is the energy level of the upper state in wave number.

Temperatures in mixtures of argon and helium or argon and hydrogen may also be determined from the same pair of Ar II lines. These measurements are valid if local thermodynamic equilibrium (LTE) is assumed. According to Bott (Ref. 34), LTE is completely established at currents over 100 A. Thus, the Ar II temperature data were fitted to a curve of the form:

$$f(r) = a_1 r^2 + a_2 \exp\left[a_3 (|r| = a_4)^2\right] + a_5$$

**Trademark of EG&G Princeton Applied Research Corporation.*

where a_j are parameters, f(r) are temperatures, and r is the radial distance from arc axis.

This form produces a curve with symmetry about the axis r = 0. Although there is no theoretical justification for choosing a curve of this form, it appears to produce a reasonable fit to the temperature data under the assumption of cylindrical geometry. It is also one of the simpler forms from a much larger set of possible forms. The computer data used to generate the fitted curve were an implementation of the algorithm described by Bevington (Ref. 35).

Ar I temperatures were determined by evaluating the following equation:

$$T = \frac{-E}{0.695\left[\ln \epsilon - \ln C \frac{\eta(T)}{u(T)}\right]}$$

where E is the energy level of the upper state, ϵ the radial intensity, $\eta(T)$ particle densities, u(T) partition function, and C a constant. Since C and u(T) are not known exactly, Ar II temperatures were used to calibrate the central Ar I intensity value for these unknowns, and the remaining temperatures were then calculated.

Results and Discussion

The results of this investigation and discussion relative to prior work are presented in the order of primary variables evaluated – gas composition, arc current, electrode (cathode) tip geometry, and anode material.

Initial measurements were made in a pure (99.999 wt-%) argon atmosphere over a water-cooled copper chill block (anode) to establish a baseline for comparison with studies by other investigators. A 2.00 mm (0.08 in.) arc length, 30 deg cathode vertex angle, and 150 A arc current were used: These conditions also provided the most stable welding arc possible without resorting to unrealistic wall or chamber-stabilized arcs used in physics experiments. The radial temperature distribution at four vertical locations in this arc is given in Fig. 4.

Since a freshly ground tungsten electrode was used for each set of experimental conditions, the effect of electrode service time on temperature and repeatability was questioned. Measurements taken at 5 minute (min) intervals during the first 15 min of operation indicate a ±3.3% variation in temperature, which is well within the measurement accuracy.

Scatter in experimental data was a function of most of the variables in this investigation. Scatter increased with increasing helium content, vertex angle, current, gap, and the presence of a molten anode. For the conditions responsible for the data in Fig. 4, scatter in spectral line intensity is generally ±1% averaged over the five repetitions of ten scans (50 individual measurements). The scatter is less, of course, near the axis due to a greater electron density for the transitions measured. A curious condition becomes obvious when the scatter in temperature is noticed to be greater (±5%) than scatter in intensity measurements. This magnification of scatter in experimental data is attributed to the Abel integral inversion (Ref. 3). The problem becomes more severe as the scatter increases for other experimental conditions.

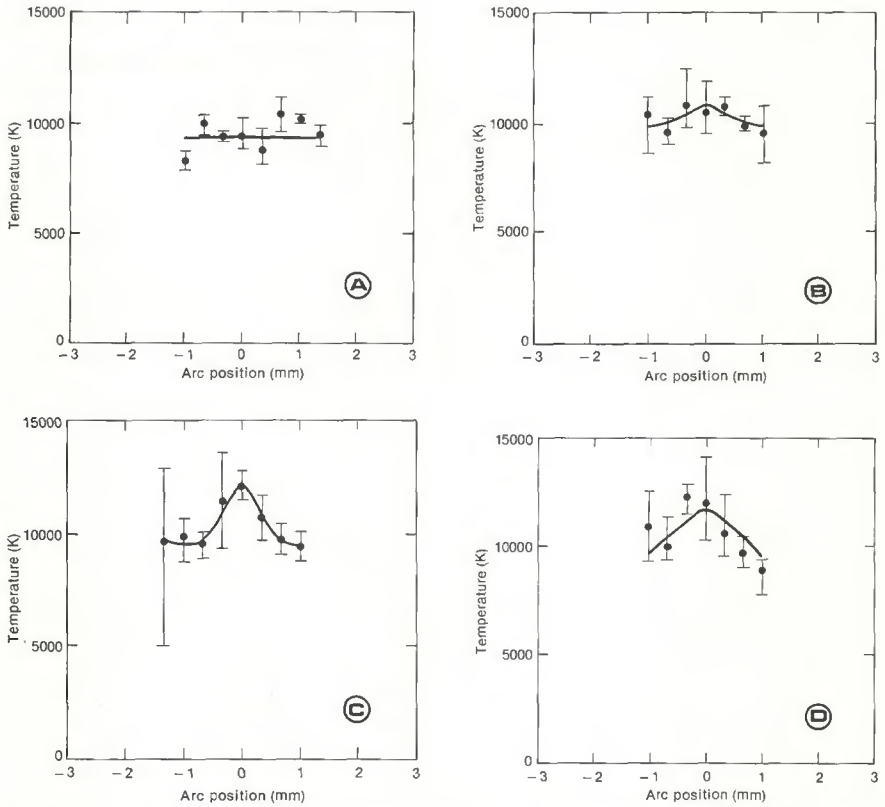

Fig. 4 – Computer curve fit for radial temperature distribution – 100% Ar, 150 A, 30 deg vertex angle: A – 0.25 mm (0.01 in.) slice; B – 0.50 mm (0.02 in.) slice; C – 1.00 mm (0.04 in.) slice; D – 1.50 mm (0.06 in.) slice

Choice of welding power supply, fortunately, had no effect on either scatter or repeatability. Power supplies from two different manufacturers had no effect on results at 150 A when both were calibrated to ±2% of set current. Data from one power supply did exhibit more background noise at 300 A than the other.

Data presented in Fig. 4 indicate that the radial temperature distribution develops an axial peak, and that peak temperature increases with increasing distance from the cathode up to the midpoint of the gap. Peak temperatures for these conditions are near 12,000 K and drop to approximately 10,000 K at a radius of 1.0 mm (0.04 in.). The radial temperature distribution calculated from a single Ar I line agrees reasonably well with the Ar II measurements and is useful for the neutral region outside the plasma. Figure 5 (derived from Fig. 4) shows an isothermal map of the plasma.

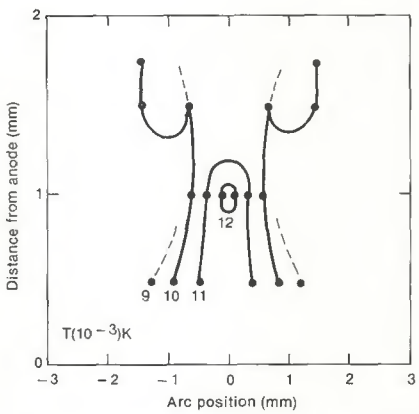

Fig. 5 – Isothermal map of arc – 100% Ar, 150 A, 30 deg vertex angle

When results are compared with prior studies, fair to excellent agreement is noted with one group of investigators (Ref. 1, 3, 4, 17), while poor agreement is noted with another group (Ref. 11, 14, 15). Both groups consisted of distinguished scientists and appear to have conducted well-designed experiments.

One clue to this disagreement emerges when the raw intensity data from this work is compared to that of Olsen (Ref. 14). The relative intensity distributions for the two studies, shown in Fig. 6, are remarkably similar, and yet the calculated temperatures do not agree well at all. Since the Abel integral inversion is a straightforward computation, it should

not be suspect unless very small differences in intensity can cause large differences in temperature as calculated by the one- and two-line methods. Another explanation may be that certain approximations inherent in Olsen's method of calibrating the Ar I intensities, such as only thermal processes being active in the central region of the 200 A arc, may have led to conclusions which resulted in large uncertainties in the arc temperatures.

The various investigators cited in this paper used a variety of arc lengths (2.0 to 12.0 mm, i.e., 0.08 to 0.47 in.) and hence significantly different arc voltages. Vinogradov (Ref. 20) suggested that temperature is a function of arc length. However, a limited investigation of a 10.0 mm (0.39 in.) arc in this work indicated little difference in the first three millimeters from the cathode tip. Below this point, the temperature dropped below that needed for Ar II excitation. Therefore, measurements presented here should agree with others using different arc lengths in regions of the arc near the cathode.

Shielding Gas Composition

When helium is added to the argon shielding gas, several interesting and somewhat disputed effects occur. Figure 7A shows the radial temperature distribution at the arc midpoint (1.00 mm, i.e., 0.04 in., slice) for a 25 wt-% argon/75 wt-% helium shielding gas composition (hereafter designated 25 Ar/75 He). Figure 7B is for a 10 Ar/90 He mixture. Although space does not permit figures for 10, 25, and 50% helium contents, changes are fairly linear up to 75% helium. Effects are significant at this level and above. Figure 7C is for the 95 Ar/5 H_2 mixture.

It has been suggested that helium should have a positive effect on arc temperature (Ref. 3, 5, 9, 11) due to its greater ionization potential (24.58 eV for He I compared to 15.76 eV for Ar I). Figures 4C, 7A and 7B clearly indicate that there is little effect on peak temperatures. If anything, temperatures decrease slightly in helium. However, helium has an enormous effect on the arc radius. For

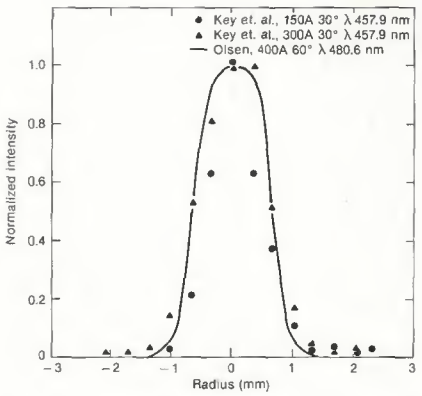

Fig. 6 — Normalized radial intensity distribution

comparison purposes arc radius is defined here as the detectable plasma radius, generally above 8,000 K (13,940°F). A 10 Ar/90 He shielding gas mixture has a plasma diameter nearly three times larger than a similar arc shielded by pure argon.

The high helium arcs are also generally isothermal as predicted by Ludwig (Ref. 11). Since this investigation, to the authors' knowledge, is the first that measures welding arc temperature in argon-helium mixtures, no comparison with prior work is possible. However, the general trends, if not the peak temperatures, are predicted by Glickstein's model (Ref. 5).

Helium's effect on radial temperature distribution can be explained by careful analysis of all of its thermophysical properties, not just ionization potential. Thermal conductivity, as suggested by Ludwig (Ref. 11), and heat capacity must be considered. At temperatures in the vicinity of 5,000 to 10,000 K (8540 to 17540°F), thermal conductivity and heat capacity for helium are nearly an order of magnitude higher than for argon.

The actual welding effects of helium are well known (Ref. 31). Deeper penetration and better fusion zone depth/width are most important. Quigley's heat transfer analysis for the GTAW process (Ref. 16) would seem to refute the effect of conductive or convective heat transfer. However, if his analysis was re-evaluated using the properties of helium, the ranking of effective heat transfer mechanisms will be altered and may explain, in part, welding effects of helium (electric field effects on fluid flow must also be considered). This argument has been offered in various forms by Ludwig (Ref. 11), Nestor (Ref. 13), Morten and Gage (Ref. 21), and Krinberg (Ref. 36). Ionization potential, at least as a controlling property, was refuted very early by Finkelnburg (Ref. 1) who noted:

"Ionization potential of an atom is lowered by the presence of a large density of electrons and ions in the surrounding plasma which furthermore influence mobility of electrons and ions in a way not accurately known."

The argon in the mixture could be the electron and ion source mentioned.

Other factors, beyond the scope of this investigation, undoubtedly contribute to welding effects of helium. Leibzon (Ref. 8), for instance, indicates that shielding gas composition has a definite effect on the presence and strength of plasma jets. These jets and other arc forces are thought to have a variety of effects on fluid flow in the weld pool and hence a significant welding influence (Ref. 37).

One mixture containing hydrogen was evaluated — 95 Ar/5 H_2 — since its penetration profiles are similar to the higher helium content mixtures — Fig. 7C. Hydrogen decreased peak temperature slightly and increased the plasma radius approximately 50%. Hydrogen's effects on welding are thought to be related to efficient recovery of its dissociation energy at the anode surface (Refs. 24, 25) and the possibility of strong plasma jets.

Arc Current

A comprehensive set of experiments was conducted at 300 A current in addition to those already cited at 150 A. A limited set was conducted at an intermediate current of 200 A.

Doubling the current from 150 to 300 A had little effect on peak temperatures but increased the plasma radius in pure

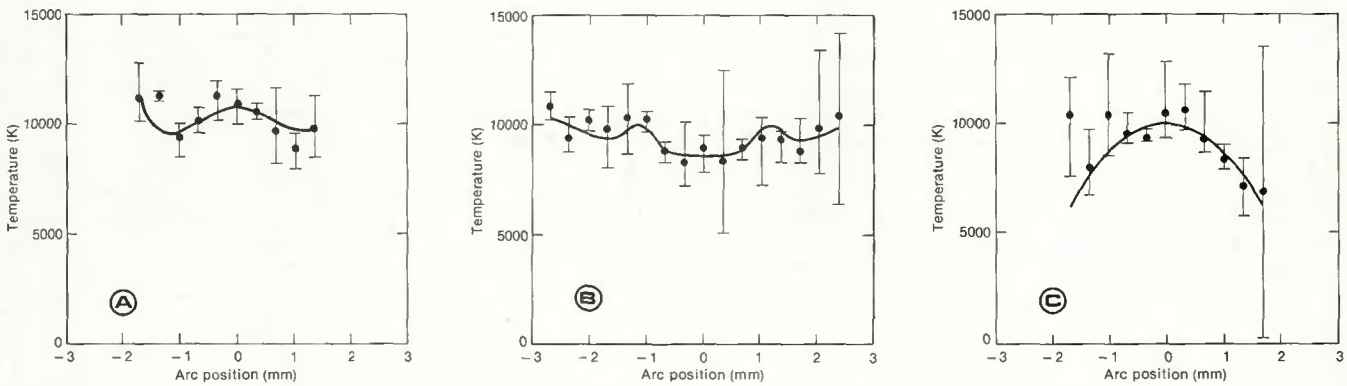

Fig. 7 — Computer curve fit for radial temperature distribution at arc midpoint (1.00 mm, i.e., 0.04 in. slice) — 150 A, 30 deg vertex angle: A — 25 Ar/75 He shielding gas; B — 10 Ar/90 He shielding gas; C — 95 Ar/5 H_2 shielding gas

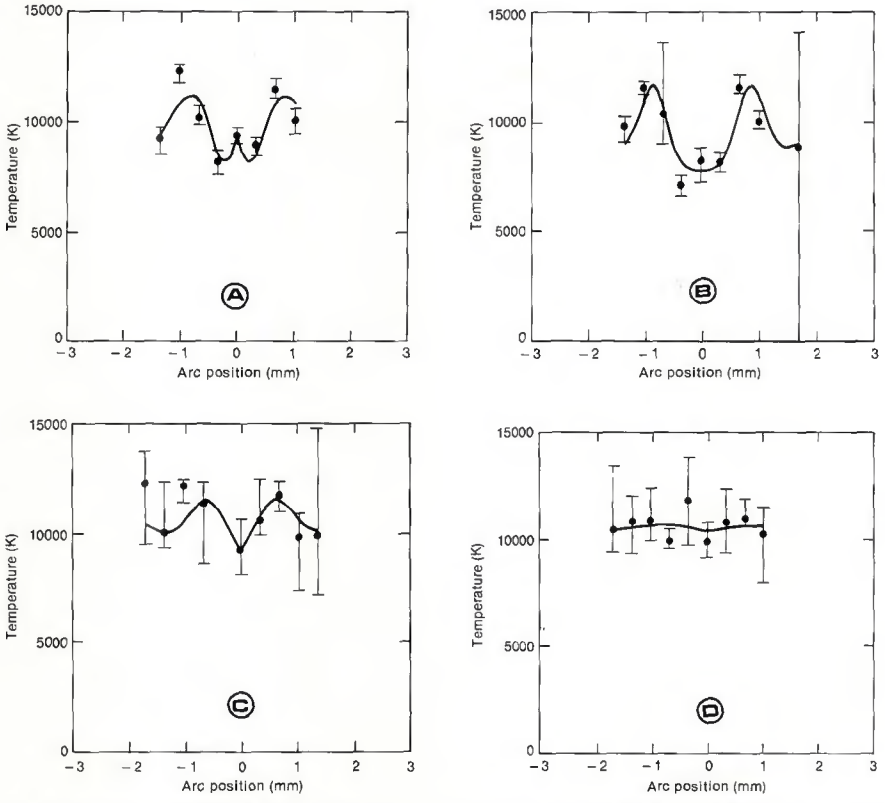

Fig. 8 — Computer curve fit for radial temperature distribution — 100% Ar, 300 A, 30 deg vertex angle: A — 0.25 mm (0.01 in.) slice; B — 0.50 mm (0.02 in.) slice; C — 1.00 mm (0.04 in.) slice; D — 1.50 mm (0.06 in.) slice

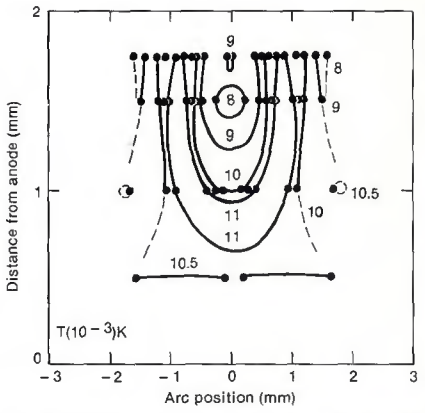

Fig. 9 — Isothermal map of arc — 100% Ar, 300 A, 30 deg vertex angle

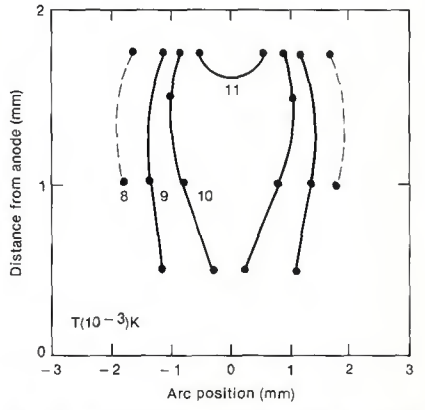

Fig. 10 — Isothermal map of arc — 100% Ar, 300 A, 90 deg vertex angle

argon and caused a significant axial temperature drop as shown in Fig. 8. This temperature drop in the upper part of the plasma disappears near the anode — Fig. 8D.

The following hypothesis is currently being evaluated: high currents induce turbulent flow, which introduces a larger quantity of relatively cool shielding gas that is subsequently heated as it flows toward the anode. This temperature dip is not seen in helium, because helium heats up faster due to its much greater thermal conductivity. An isothermal map is shown in Fig. 9. Helium and hydrogen have similar effects at 300 A as they have at 150 A.

Electrode Tip Geometry

Welding effects of electrode vertex angle in pure argon are well documented (Ref. 27-30) and were more recently reviewed relative to shielding gas composition (Ref. 31). Electrode vertex angle is an important variable under certain conditions. However, Fig. 10 shows that a 90 deg vertex angle only makes the temperature distribution slightly more diffuse (small decrease in peak temperature, small increase in plasma radius).

The effect of vertex angle on temperature is in agreement with Petrie and Pfender (Ref. 15). Larger vertex angles do increase scatter slightly and may be more effective in constricting high helium content arcs.

Anode Material

The results from experiments conducted over a moving molten pool were quite similar to results of stationary arcs on a nonmolten copper chill block for both 150 and 300 A currents. Molten pool effects are confined to a region less than 0.50 mm (0.02 in.) from the surface. Low temperatures and a resulting loss of local thermodynamic equilibrium make accurate quantitative measurements in this region virtually impossible by emission spectroscopy methods.

Variables considered in this work do influence loss of metal vapors from the pool. However, this topic is the subject of other investigations.

Conclusions

The foregoing results and discussion from an investigation of the influence of primary welding variables on radial temperature distribution in the GTAW process support the following conclusions:

1. Shielding gas composition has a significant effect on plasma diameter and radial temperature distribution. It has an insignificant effect on peak temperature. Further work is required to accurately model heat flow in an arc shielded by gas mixtures.

2. Electrode (cathode) vertex angle has a negligible effect on peak temperature and radial temperature distribution.

3. A large increase in arc current generally causes little change in peak temperature but does cause an increase in plasma diameter, especially in pure argon.

4. The effects of a molten anode are confined to a region less than 0.50 mm (0.02 in.) above the surface — a region that is difficult to measure by emission spectroscopy. Although data exhibits more scatter, trends are similar to nonmolten anode studies.

5. Arc length has no appreciable influence on temperature measurements in these experiments.

Acknowledgments

Appreciation is extended to L. D. Reynolds for his contributions in optics and experimental measurements.

The work discussed in this paper was supported by the U.S. Department of Energy, Office of Energy Research, Office of Basic Energy Sciences, under DOE Contract No. DE-AC07-76ID01570.

References

1. Finkelnburg, W. 1949 (Oct.). The high current carbon arc and its mechanism. *Journal of Applied Physics* 20:468-474.

2. Frolov, V. V. 1954. Physico-chemical processes in the welding arc. Mashgiz.

3. Gick, A. E. F., Quigley, M. B. C., and Richards, P. H. 1973. The use of electrostatic probes to measure the temperature profiles of welding arcs. *J. Phys. D: Appl. Phys.* 6:1941-1949.

4. Glickstein, S. S. 1976. Temperature measurements in a free burning arc. *Welding Journal* 55 (8):222-s to 299-s.

5. Glickstein, S. S. 1979. Arc modelling for welding analysis. *International conference proceedings on arc physics and weld pool behavior*:1-6. London, England: The Welding Institute.

6. Kobayashi, M. and Suga, T. 1979. A method for the spectral temperature measurements of a welding arc. *International conference proceedings on arc physics and weld pool behavior*:25-37. London, England: The Welding Institute.

7. Khrenov, K. K. 1949. *The electric welding arc*. Mashgiz.

8. Leibzon, V. M., Glushko, V. Ya., and Frolov, V. V. 1977. The energy and technological parameters of arc running between a non-consumable electrode and a copper plate in argon, nitrogen or helium. *Svar. Proiz.*, 8:9-11.

9. Leskov, G. I. 1967. The progress of research on the physics and technology of electric arc welding in the USSR. *Svar. Proiz.*, 11, 10-13.

10. Leskov, G. I. 1963. Approximate equations for calculating the characteristics of various welding arcs. *Auto. Weld.* 16:5.

11. Ludwig, H. C. 1959. Plasma-energy transfer in gas shielded welding arcs. *Welding Journal* 38(7):296-s to 300-s.

12. Mills, G. S. 1977. Use of emission spectroscopy for welding arc analysis. *Welding Journal* 56(3):93-s to 96-s.

13. Nestor, O. H. 1962 (May). Heat intensity and current density distributions at the anode of high current inert gas arcs. *Journal of Applied Physics* 33:1638-1648.

14. Olsen, H. N. Thermal and electrical properties of an argon plasma. *The Physics of Fluids* 2 (6):614-623.

15. Petrie, T. W. and Pfender, E. 1970. The influence of the cathode tip on temperature and velocity fields in a gas-tungsten arc. *Welding Journal* 49(12):588-s to 596-s.

16. Quigley, M. B. C., Richards, P. H., Swift-Hook, D. T., and Gick, A. E. F. 1973. Heat flow to the workpiece from a TIG welding arc. *J. Phys. D: Appl. Phys.* 6:2250-2258.

17. Seeger, G., and Tiller, W. 1979. Laser diagnostics on the TIG arc. *Proceedings of international conference on arc physics and weld pool behavior*. London, England: The Welding Institute, 315-326.

18. Shaw, C. B., Jr. 1975 (Feb.). Diagnostic studies of the GTAW arc—Part 1. *Welding Journal* 54(2):33-s to 44-s.

19. Shaw, C. B., Jr. 1975 (March). Diagnostic studies of the GTAW arc—Part 2. *Welding Journal* 54(3):81-s to 86-s.

20. Vinogradov, V. A., Popenko, U. S., Guma, V. V. 1974. Controlling welding parameters by spectral analysis methods. *Weld. Proiz.* 21(12), 8-10.

21. Kuhn, W. E., ed. 1956 (April 30, May 1) *Arcs in inert atmospheres and vacuum*, pp. 8-10.

22. Theirs, R. E., and Vallee, B. L. 1956. The effect of noble gases on the characteristics of the D. C. arc. *Colloquim spectroscopicum internationale VI*:179-185.

23. Vallee, B. L., and Adelstein, S. J. 1952 (May). The effects of argon and argon-helium mixtures on the direct current arc. *Journal of the Optical Society of America* 42:295-299.

24. Ikonomov, N., Pavlovic, B., Vukanovic, V., and Rakicevic, N. 1971. The effect of the plasma composition on characteristics of the d-c arc—III, argon in carbon dioxide. *Spectrochimica acta*, 26B, 117-121.

25. Vukanovic, V., Ikonomov, N., and Pavolic, B. 1971. The effect of the plasma composition on characteristics of the D. C. arc—I general discussion of the effect of the chemical reactions, *Spectrochimica Acta*, 26B:95-108.

26. Erokhin, A. A., Bukarov, V. A., and Ischenko, Yu. S. 1971. Influence of tungsten cathode geometry on some welding arc characteristics and metal penetration. *Weld. Prod.* 18(12) 25-28.

27. Savage, W. F., Strunck, S. S., and Ishikawa, Y. 1965. The effect of electrode geometry in gas tungsten-arc welding. *Welding Journal* 44 (10):489-s to 496-s.

28. Chihoski, R. A. 1968. The effects of varying electrode shape on arc, operations, and quality of welds in 2014-T6 aluminum. *Welding Journal* 47 (5):69-s to 82-s.

29. Spiller, K. R., and Mac Gregor, G. J. 1970. Effect of electrode vertex angle on fused weld geometry in TIG-welding. *Proceedings of the conference on advances in weld processes*:82-88. Cambridge, England: The Welding Institute.

30. Glickstein, S. S., Friedman, E., and Yeniscavich, W. 1975. Investigation of alloy 600 welding parameters. *Welding Journal* 54 (4):113-s to 122-s.

31. Key, J. F. 1980. Anode/cathode geometry and shielding gas interrelationships in GTAW. *Welding Journal* 59 (12):364-s to 370-s.

32. Lochte-Holtgreven, W. 1968. *Plasma diagnostics*:178-218 New York: American Elsevier.

33. Barr, W. L. 1962. Method for computing the radial distribution of emitters in a cylindrical source. *J. Opt. Soc. Am.* 52:885-888.

34. Bott, J. F. 1966. Spectroscopic measurement of temperature in an argon plasma arc. *Phys. Fluids* 9:1540-1547.

35. Bevington, P. R. 1969. *Data reduction and error analysis for the physical sciences:* Chap. 11, pp. 204-246. New York: McGraw-Hill, Inc.

36. Krinberg, I. A. On the theory of an electric columnar arc burning under conditions of natural convection (1), *Soviet-Physics—Technical Physics* 9 (5):684-689.

37. Mills, G. S. 1979. Fundamental mechanisms of penetration in GTA welding. *Welding Journal* 58 (1):21-s to 24-s.

WRC Bulletin 284
April, 1983

The External Pressure Collapse Tests of Tubes

by E. Tschoepe and J. R. Maison

An experimental program was performed to confirm or refute the applicability of Figure UG-31 in Section VIII, Division 1 of the ASME Boiler and Pressure Vessel Code to the design of tubes under external pressure. Commercially available tubes were subjected to external pressure until collapse occurred. The data generated indicates the current ASME design rules for tubes under external pressure are suitable for continued application.

Publication of this report was sponsored by the Subcommittee on Shells of the Pressure Vessel Research Committee of the Welding Research Council.

The price of WRC Bulletin 284 is $12.00 per copy, plus $5.00 for postage and handling. Orders should be sent with payment to the Welding Research Council, Room 1301, 345 East 47th St., New York, NY 10017.